Automated Damage Assessment of Critical Infrastructure Using Online Mapping Technique with Small Unmanned Aircraft Systems

Zhong Mao
Electrical and Computer Engineering Department
Northeastern University
Boston, USA
zmao@coe.neu.edu

Yujie Yan
Civil and Environmental Engineering Department
Northeastern University
Boston, USA
yan.yuj@husky.neu.edu

Jiahao Wu
Electrical and Computer Engineering Department
Northeastern University
Boston, USA
wu.jiaha@husky.neu.edu

Jerome F. Hajjar
Civil and Environmental Engineering Department
Northeastern University
Boston, USA
jf.hajjar@neu.edu

Taşkın Padır
Electrical and Computer Engineering Department
Northeastern University
Boston, USA
t.padir@northeastern.edu

***Abstract*—Rapid inspection and assessment of critical infrastructure after man-made and natural disasters is a matter of homeland security. The primary aim of this paper is to demonstrate the potential of leveraging small Unmanned Aircraft System (sUAS) in support of the rapid recovery of critical infrastructure in the aftermath of catastrophic events. We propose our data collection, detection and assessment system, using a sUAS equipped with a Lidar and a camera. This method provides a solution in fast post-disaster response and assists human responders in damage investigation.**

***Index Terms*—sUAS, Infrastructure Inspection**

I. Introduction

Both natural events and potential terrorist attacks will disrupt normal operations of lifeline infrastructure sectors, which is of great significance to homeland security. Consequently, rapid response and recovery capabilities would clearly benefit from leveraging a growing interest by major infrastructure owners and operators in using autonomous or human-supervised technological assets to support the inspection and maintenance of infrastructure. For example, railroad operators have been experimenting with the use of human-supervised sUAS to conduct remote examination of the condition of their rail tracks to support routine maintenance and repair. These same assets have the potential to be repurposed in the aftermath of a disaster to assess disaster sites to detect infrastructure damage and to support data-driven decision making processes at emergency response centers. This project envisions that sUAS can serve as an ubiquitous tool for emergency management teams in the near future.

Recently, the use of sUAS in infrastructure inspection is an active eld of research. sUAS has been used in bridge [6], building facades inspection [7] using a RGB camera or stereo camera [9], and general visual inspection [11]. As point cloud map gives a direct vision in geometry and size [12], it can be used to identify the damage on infrastructure

978-1-7281-5092-5/19/$31.00 ©2019 IEEE

[10], such as power line inspection [8] using laser scanner.

However, primary damage detection work is based on post-data processing and the online mapping result is not accurate enough due to limited onboard data processing capability. In this paper, we propose to provide an integrated sUAS-sensor system that will assist in rapid damage assessment in a post-disaster scenario under human supervision. The sUAS, equipped with Lidar and camera, is able to collect point cloud and image data that represent 3D geometric and textural information of the environment. In our case, sUAS will produce an online point cloud map, from which the damage can be visually recognized, that is potential to apply damage detection algorithm. In addition to the previous work that is introduced in [1], we have improved our online mapping algorithm to improve the mapping accuracy and developed an image-based concrete crack detection algorithm.

The paper is organized as follows. The system is introduced in section II and the methodology in section III, including online mapping algorithm, image-based crack detection and sUAS control scheme. After that, the experimental results and algorithm validation are presented in section IV.

II. System Overview

In this project, the sUAS-sensor system we use is developed based on the system we used in [1]. Recall that DJI M600 Pro is selected as aerial platform and Velodyne VLP16 as Lidar sensor. In our previous design, we set the gimbal to rotate at a constant speed, and the angle of gimbal is expected to grow uniformly. Actually, the constant gimbal speed can't be guaranteed in field tests, especially when the sUAS is tilt. Thus we add an encoder to obtain the rotary angle of the gimbal axis, which is illustrated in Fig. 1(a). We also equipped a camera next to the Lidar, which is shown in Fig. 1(b). The gimbal of camera is able to pitch from $+30°$ to $-90°$, and yaw within $\pm 320°$. A soft damper is designed to connect the sUAS frame and the camera mounting plate, so that the image blurring is reduced due to shock absorption.

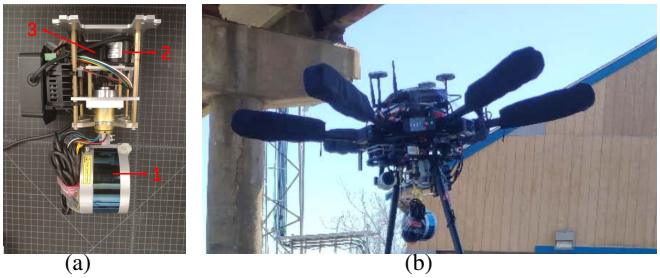

(a) (b)

Fig. 1. a) The Lidar 1, the encoder 2 and the motor 3; b) DJI Z3 camera.

III. Methodology

Our methodology is consisted of sUAS on-board and post-flight data processing. Some previous work has been introduced in [1], including Lidar gimbal calibration, sUAS path planning and Lidar based post-flight damage detection. In this section, we will focus on the online mapping and the image based damage detection.

A. Online Mapping

Our SLAM algorithm is developed based on [3], which aims to provide a clear and accurate online map for infrastructure damage detection in real time. The mapping, or point cloud registration process can be simply viewed as merging all scans into a fixed coordinate, which is set to be the Lidar frame of the first scan. The Lidar spins internally at a rate of 600 rpm and raw point cloud is described in the Lidar frame, no matter when and where it is. The Lidar returns point cloud flow at 10Hz, and

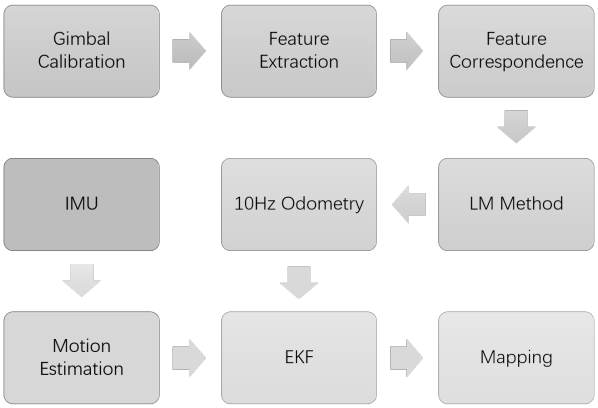

Fig. 2. Flow chart of online mapping.

the efficiency of mapping relies on the point cloud size, which makes it difficult to register all raw point

978-1-7281-5092-5/19/$31.00 ©2019 IEEE

cloud data in online mapping. A brief flow of the online mapping process is depicted in Fig. 2 and the algorithm is displayed in Fig. 3 where P_k and $P_{k+1}$is

Algorithm 1 Online mapping

Input:
Scan P_k and P_{k+1} at time stamp t_{k+1} and t_{k+2};
Output:
Transformation T_k and map P;

if at the beginning of mapping **then**
$P = 0$ and $T_k^L = 0$
end if
Update $P_k = P_k * T_k^E$ using encoder;
Select edge and planar points as feature points, and then construct correspondence for each feature point;
for a number of iterations **do**
Solve the non-linear correspondence equations using LM method, and update T_k^L;
end for
if IMU information is available **then**
Estimate the motion of sUAS using IMU and generate T_k^I, and update $T_k = EKF(T_k^L, T_k^I)$ using EKF;
else
$T_k = T_k^L$
end if
Update map $P = P + P_k * T_k$

Fig. 3. Online mapping algorithm.

the point cloud scan at time stamp t_k and t_{k+1}; while T_k and P are the transformation from sUAS frame to fixed frame of each scan and accumulated point cloud map respectively. The transformation from Lidar frame to sUAS frame using encoder, from sUAS frame to world fixed frame using Lidar and Inertial Measurement Unit (IMU), are denoted as T_k^E, T_k^L and T_k^I respectively. Firstly, we integrate each scan from Lidar frame to sUAS frame using our gimbal calibration method [1], in which the axis angle ωt term can be replaced by encoder reading directly. This is similar to coarse registration and the transformation matrix is derived using Eq.3 in [1].

Taking advantage of the gimbal calibration, each point cloud is projected close to the actual pose, without which, the feature-matching based iteration algorithm may result in local optimum or divergency, especially in feature-less environment. Recall that we use a 16 channel Lidar, which covers a view of 30° vertically, and we classify and save all points into 16 sequences according to the relative vertical angle in Lidar frame within each scan. Similarly, the points in the same sequence will be sorted by time, which can be derived by relative horizontal angles. The outliers and the points belong to none of the 16 sequences will be removed. After that, we need to extract the feature points that can be represent the full scan. We go over all the points in the same sequence and resort based on the curvatures [3]. The points with curvature over the upper threshold as edge points and below the lower threshold as planar points. Then, we choose the closest point to the edge point to form an edge line as its correspondence and generate planar patch as a correspondence to a planar point. After that, Levenberg-Marquardt (LM) method is applied to solve the nonlinear correspondences transformation equations, which is similar to Iterative Closest Point (ICP) method, and the results can be represented as sUAS pose transformation between 2 consecutive scans. At this point, we derive the Lidar odometry at 10Hz. To enhance the reliability of the transformation, we integrate IMU motion estimation result with Lidar odometry using an Extended Kalman Filter (EKF) [5]. After that, we project each point cloud full scan onto the fixed frame and update the map sequentially.

B. Image Based Damage Detection

Concrete cracks are one of the most common surface damage in major structural elements. Due to their sizes, they usually cannot be captured by a mobile laser scanner. As such, this project focuses on detecting concrete cracks through processing the image sequences acquired by the camera. The proposed crack detection module contains three main steps: 1) detect the individual concrete elements from the point cloud map using the method introduced in [1]; 2) identify the region-of-interest (ROI) in each image by fusing the images with point cloud map; 3) formulate image patches from the ROIs and identify image patches that contain cracks using a classifier that is trained based on convolution neural network (CNN). To train the classifier, 55000 128x128 image patches, that cover a wide range of crack patterns, crack width, background textures and illuminations, were collected and labelled. Among the 55000 image patches, 23500 of them are crack images and 31500 of them are non-crack images. 80% of the image patches were used for training and 20% were used for validation. The architecture of the CNN network, which is developed based

978-1-7281-5092-5/19/$31.00 ©2019 IEEE

upon VGG network [4], consists of 6 convolution layer, 3 pooling layer, 1 fully-connected layer. The final training accuracy is 98.51 % and the validation accuracy is 98.32 %.

C. sUAS control scheme

Within the scope of the project, we developed both human-in-the-loop and semi-autonomous control algorithms for the sUAS. The prerequisite for a successful flight to obtain accurate sensor data relies on stabilizing the position and attitude of the sUAS. This is a challenging task especially when there is significant external disturbance present during the flight caused primarily by the weather conditions. Navigation in indoor environments suffer from the lack of GPS signal hence the localization needs to rely on the IMU based estimation algorithms. GPS information can be used to evaluate the localization confidence together with IMU in outdoor missions. As we continue to develop our navigation algorithms, we relied on validation in simulation environments in Fig. 4. Under human operation, a remote controller is used to send flight command and receive messages from sUAS via wireless telecommunication. In autonomous flight mode, the sUAS is programmed to follow a predesigned trajectory, for example, a path that goes around the interesting location so that the scanning of complete external structure information can be covered.

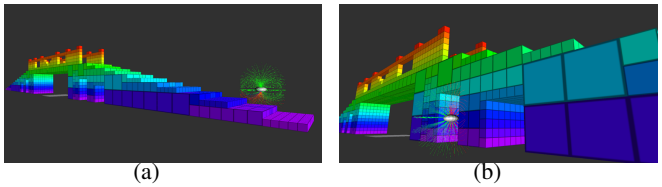

(a) (b)

Fig. 4. Validation of autonomous path planning algorithms around a bridge in the simulation environment. Our work continues with the implementation of this algorithm on the actual platform.

IV. Experimental Procedures and Validation of Algorithms

Our based damage detection is validated in an outdoor netted enclosure [1] and the online mapping algorithm is validated both during a bridge inspection experiment and inside of the netted enclosure.

A. Online mapping results

The first experiment is tested in the netted enclosure using the same scenario in Fig.9a in [1]. As we can see from Fig. 5 that the holes are visually recognizable from online map. The second

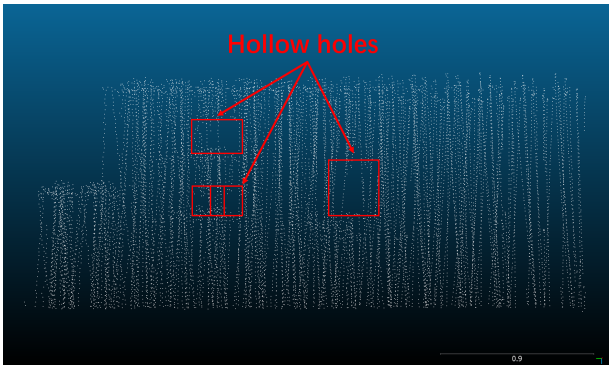

Fig. 5. The wall extracted from the online map and the hollow areas are labeled.

experiment is tested during the inspection of a real bridge. The sUAS is placed stationarily on ground in front of the bridge before take off. Then, the sUAS takes off and arises to 4 meters high and hover at that altitude for 30 seconds. After that, the sUAS flies under across the bridge between two piers and lands on the other side of the bridge. The online map of the bridge is depicted in Fig. 6(a) and the partial bridge is segmented out and displayed in Fig. 6(b). A typical damage, concrete spalling, is located on the pier in Fig. 7(a) and the spalling is visually recognizable on the pier extracted from the online map in Fig. 7(b).

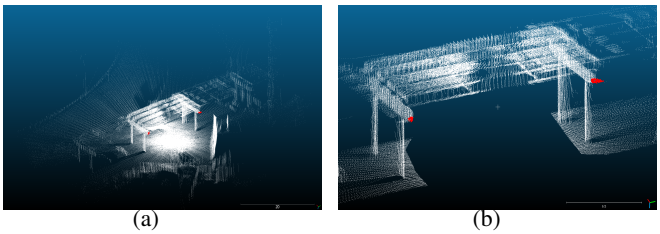

(a) (b)

Fig. 6. a) The online map of the bridge and the surrounding area; b) the bridge is segmented out for explicit visualization and the concrete spallings are marked as red.

B. Image based Crack Detection

The image-based crack detection algorithm is illustrated using an example as shown in 8. The

978-1-7281-5092-5/19/$31.00 ©2019 IEEE

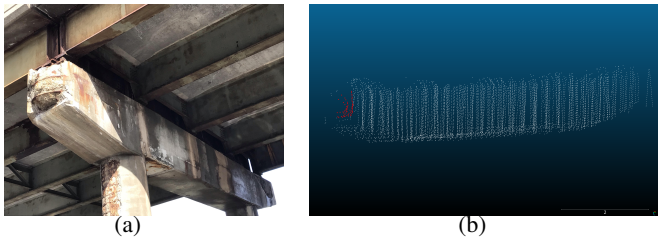

(a) (b)

Fig. 7. a) The actual concrete spalling on the pier; b) the spalling area is visually recognizable and marked as red on the pier extracted from the online map.

image is taken from the concrete pier of a in-service bridge where microscale cracks can be observed. In this example, the concrete pier is identified as the object-of-interest in the point cloud map manually. According to the object-of-interest, the ROIs in the image is computed and image patches are generated automatically (Fig. 8(a)). The image patches are then processed by the trained classifier to identify crack image patches as shown in Fig. 8(b) and Fig. 8(c). The results indicate that both ROIs and crack image patches can be identified correctly.

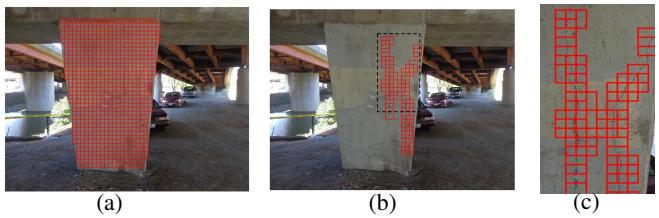

(a) (b) (c)

Fig. 8. a) Image patches generated from the ROIs; b) crack image patches identified by the classifier; c) Zoom-in view of the crack image patches .

V. Conclusion and Future Work

Our sUAS-sensor system is verified of the capability of environmental mapping and damage detection for both online and offline cases. We will validate the mapping and damage detection algorithms under a fully autonomous flight that the sUAS will navigate to targets of interest perceived automatically. We'll also improve the accuracy of the online mapping algorithm so that more damage types can be detected.

Acknowledgment

This research was supported by the Pacific Northwest Economic Region with funding from the Department of Homeland Security as part of the National Infrastructure Protection Plan (NIPP) Security and Resilience Challenge and the Northeastern University's Global Resilience Institute seed funding program.

References

[1] Mao Z, Yan Y, Wu J, et al. Towards Automated Post-Disaster Damage Assessment of Critical Infrastructure with Small Unmanned Aircraft Systems[C]//2018 IEEE International Symposium on Technologies for Homeland Security (HST). IEEE, 2018: 1-6.

[2] Zhang L, Yang F, Zhang Y D, et al. Road crack detection using deep convolutional neural network[C]//2016 IEEE international conference on image processing (ICIP). IEEE, 2016: 3708-3712.

[3] Zhang J, Singh S. LOAM: Lidar Odometry and Mapping in Real-time[C]//Robotics: Science and Systems. 2014, 2: 9.

[4] Simonyan K, Zisserman A. Very deep convolutional networks for large-scale image recognition[J]. arXiv preprint arXiv:1409.1556, 2014.

[5] Opromolla R, Fasano G, Rufino G, et al. LIDAR-inertial integration for UAV localization and mapping in complex environments[C]//2016 International Conference on Unmanned Aircraft Systems (ICUAS). IEEE, 2016: 649-656.

[6] Lattanzi, David, and Gregory R. Miller. "3D scene reconstruction for robotic bridge inspection." Journal of Infrastructure Systems 21.2 (2014): 04014041.

[7] Roca, D., et al. "Low-cost aerial unit for outdoor inspection of building faades." Automation in Construction 36 (2013): 128-135.

[8] Ax, Markus, et al. "UAV based laser measurement for vegetation control at high-voltage transmission lines." Advanced Materials Research. Vol. 614. Trans Tech Publications, 2013.

[9] Omari, Sammy, et al. "Visual industrial inspection using aerial robots." Proceedings of the 2014 3rd International Conference on Applied Robotics for the Power Industry. IEEE, 2014.

[10] Stoyanov, Todor, Martin Magnusson, and Achim J. Lilienthal. "Point set registration through minimization of the l 2 distance between 3d-ndt models." 2012 IEEE International Conference on Robotics and Automation. IEEE, 2012.

[11] Morgenthal, G., and N. Hallermann. "Quality assessment of unmanned aerial vehicle (UAV) based visual inspection of structures." Advances in Structural Engineering 17.3 (2014): 289-302.

[12] Fridovich-Keil, David, Erik Nelson, and Avideh Zakhor. "AtomMap: A probabilistic amorphous 3D map representation for robotics and surface reconstruction." 2017 IEEE International Conference on Robotics and Automation (ICRA). IEEE, 2017.